

# Application of regional meteorology and air quality models based on MIPS and LoongArch CPU Platforms

Zehua Bai<sup>1,2</sup>, Qizhong Wu<sup>1,2</sup>, Kai Cao<sup>1,2</sup>, Yiming Sun<sup>3</sup>, Huaqiong Cheng<sup>1,2</sup>

<sup>1</sup>College of Global Change and Earth System Science, Faculty of Geographical Science, Beijing Normal University, Beijing 100875, China.

<sup>2</sup>Joint Center for Earth System Modeling and High Performance Computing, Beijing Normal University, Beijing 100875, China.

<sup>3</sup>Beijing Institute of Talent Development Strategy, Beijing 100032, China.

**Correspondence:** Qizhong Wu ([wqizhong@bnu.edu.cn](mailto:wqizhong@bnu.edu.cn))

**Abstract.** The Microprocessor without interlocked piped stages (MIPS) and LoongArch are Reduced Instruction Set Computing (RISC) processor architectures, which have advantages in terms of energy consumption and efficiency. There are few studies on the application of MIPS and LoongArch CPUs in the geoscientific numerical models. In this study, Loongson 3A4000 CPU platform with MIPS64 architecture and Loongson 3A6000 CPU platform with LoongArch architecture were used to establish the runtime environment for the air quality modelling system Weather Research and Forecasting–Comprehensive Air Quality Model with extensions (WRF-CAMx), in Beijing-Tianjin-Hebei region. The results show that the relative errors for the major species (NO<sub>2</sub>, SO<sub>2</sub>, O<sub>3</sub>, CO, PNO<sub>3</sub> and PSO<sub>4</sub>) between the MIPS and X86 benchmark platform are within ±0.1%. The maximum Mean Absolute Error (MAE) of major species ranged to 10<sup>-2</sup> ppbV or μg m<sup>-3</sup>, the maximum Root Mean Square Error (RMSE) ranged to 10<sup>-1</sup> ppbV or μg m<sup>-3</sup>, and the Mean Absolute Percentage Error (MAPE) remained within 0.5%. The CAMx takes about 195 minutes on Loongson 3A4000 CPU, 71 minutes on Loongson 3A6000 CPU and 66 minutes on Intel Xeon E5-2697 v4 CPU, when simulating a 24h-case with four parallel processes using MPICH. As a result, the

删除的内容: MIPS processor architecture is a type

删除的内容: of

删除的内容: has

删除的内容: was

删除的内容: WRF-CAMx

删除的内容: The CAMx takes about 15.2 minutes on Loongson 3A4000 CPU and 4.8 minutes on Intel Xeon E5-2697 v4 CPU, when simulating a 2h-case with four parallel processes using MPICH.

39 single-core computing capability of Loongson 3A4000 CPU for the WRF-CAMx  
40 modeling system is about one-third of Intel Xeon E5-2697 v4 CPU [and Loongson](#)  
41 [3A6000 CPU is slightly lower than Intel Xeon E5-2697 v4 CPU](#), but the thermal design  
42 power (TDP) of Loongson 3A4000 is [40W, while the Loongson 3A6000 is 38W](#), only  
43 about [one-fourth](#) of Intel Xeon E5-2697 v4, [whose](#) TDP is 145W. The results also verify  
44 the feasibility of cross-platform porting and the scientific usability of the ported model.  
45 This study provides a technical foundation for the porting and optimization of  
46 numerical models based on MIPS, [LoongArch](#) or other RISC platforms.

删除的内容: 30

删除的内容: one-fifth

删除的内容: which

删除的内容: Thus, Loongson 3A4000 has higher energy efficiency in the application of the WRF-CAMx modeling system.

47

## 48 1 Introduction

49 In the recent years, with the increasing demand for high-performance computing  
50 resources and rapid development in the computer industry, especially supercomputer,  
51 central processing unit (CPU) has undergone significant advancements in logical  
52 structure, operational efficiency, and functional capabilities, making it the core  
53 component of current computer technology development. There are two main types:  
54 one is complex instruction set computer (CISC) CPU (George, 1990; Shi, 2008), mainly  
55 using X86 architecture, representative vendors including Intel, AMD, etc., and widely  
56 used in high-performance computing platforms. The other is reduced instruction set  
57 computer (RISC) CPU (Mallach, 1991; Liu et al., 2022), mainly using ARM, MIPS,  
58 RISC-V and other architectures, representative vendors including Loongson, etc., and  
59 mainly used in high-performance computing platforms, which have high efficiency,  
60 excellent stability and scalability. The Microprocessor without interlocked piped stages  
61 (MIPS) architecture is one of the significant representatives of RISC architecture. MIPS  
62 was originally developed in the early 1980s by Professor Hennessy at Stanford  
63 University and his group (Hennessy et al., 1982). The simplicity of the MIPS instruction  
64 set contributes to its ability to process instructions quickly, thus achieving higher  
65 performance even in low-power conditions. In 1999, MIPS Technology Inc. released  
66 the MIPS32 and MIPS64 architecture standard (MIPS Technology Inc., 2014).  
67 Compared to the CISC CPUs, RISC CPUs demonstrate excellent performance and

74 power efficiency, which have gained popularity among chip manufacturers.

75 The Loongson processor family developed by Loongson Technology is mainly  
76 designed using MIPS architecture and Linux operating system (Hu et al, 2011), which  
77 has rich application tools in Linux open-source projects. The main reason that currently  
78 restricts the development of CPUs that implement non-X86 instruction set architecture  
79 such as MIPS64 is the immature software ecosystem (Hu et al., 2016). Based on the  
80 strategy of open-source software, Loongson platform has gained abundant software  
81 tools, making it possible to further develop scientific computing and numerical models.

82 Air quality model (AQM) systems use mathematical equations and algorithms to  
83 simulate and predict the pollutant concentration in the atmosphere. The current AQMs  
84 have become more complex, incorporating numerous factors such as emissions from  
85 industrial sources, vehicle traffic, and natural sources, as well as meteorological  
86 conditions, including modeling meteorology, emissions, chemical reactions, and  
87 removal processes (Zhang et al., 2012). Regional-scale AQMs have been widely used  
88 to predict air quality in cities, formulate emission reduction strategies, and evaluate the  
89 effectiveness of control policies (Wang et al., 2023), including the Community  
90 Multiscale Air Quality (CMAQ) modelling system (Appel et al., 2017; Appel et al.,  
91 2021), the Comprehensive Air Quality Model with extensions (CAMx; RAMBOLL  
92 ENVIRON Inc., 2014), and the Nested Air Quality Prediction Modeling System (Wang  
93 et al., 2006; Chen et al., 2015). Due to the requirement of meteorological input,  
94 commonly used offline meteorological models such as WRF (Michalakes et al., 2001)  
95 are coupled offline with the regional AQMs to provide meteorological and chemical  
96 forecast as the WRF-AQM modeling system, such the WRF-CMAQ modeling system  
97 (Wu et al., 2014).

98 Both the meteorological and air quality numerical simulation rely heavily on high-  
99 performance computing systems. The WRF-AQM systems can run stably on high-  
100 performance computing platforms based on X86 or X86-compatible instruction set  
101 architecture (ISA) CPUs, which account for the highest percentage among the main  
102 processors of current high performance computing platforms. There are relatively  
103 limited researches on the application of WRF-AQM system on MIPS [and LoongArch](#)

104 CPU platforms at present, this study focuses on the application of WRF-CAMx model  
105 on Loongson CPU platform based on the MIPS [and LoongArch](#) architectures. A  
106 simulation case covering the Beijing-Tianjin-Hebei region was set up to evaluate the  
107 differences and performance between MIPS and X86 platforms. This study validated  
108 the stability of scientific computing on MIPS [and LoongArch](#) CPU platform, and it  
109 offered technical references and evaluation methods for the porting and application of  
110 numerical models on non-X86 platforms.

删除的内容:

111 Section 2 provides the model descriptions of the Weather Research and  
112 Forecasting–Comprehensive Air Quality Model with extensions (WRF-CAMx)  
113 modeling system, and the descriptions of MIPS [, LoongArch and benchmark platforms](#).  
114 The configuration of the air quality numerical simulation system and simulation case  
115 are also presented in Section 2. Section 3 describes porting and optimization of the  
116 WRF-CAMx modelling system on MIPS [and LoongArch](#) CPU platforms. Section 4  
117 analyzes the differences of model results between MIPS CPU platform and the  
118 benchmark platform. Section 5 discusses MIPS [and LoongArch](#) CPUs performance in  
119 scientific computing. The conclusions are presented in Section 6.

删除的内容: The remainder is organized as follows.

删除的内容: platform

删除的内容: both

删除的内容:

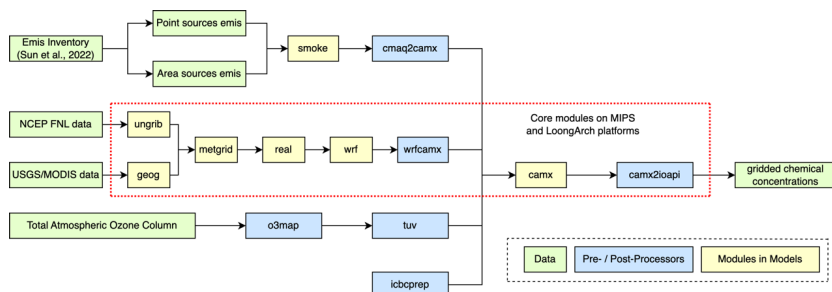
删除的内容: CPU

删除的内容: and benchmark platform

120

## 121 2 Model and Porting Platform Description

122 The air quality modeling system was constructed using the WRF v4.0 model  
123 developed by National Center for Atmospheric Research (NCAR) (Skamarock et al.,  
124 2019), and the CAMx v6.10 developed by Ramboll Environment (RAMBOLL  
125 ENVIRON Inc., 2014), as shown in Figure 1. And the Loongson 3A4000 CPU platform  
126 was chosen for the porting work in the study. This study introduced the porting of WRF-  
127 CAMx modeling system to MIPS [and LoongArch](#) CPU platforms.



135

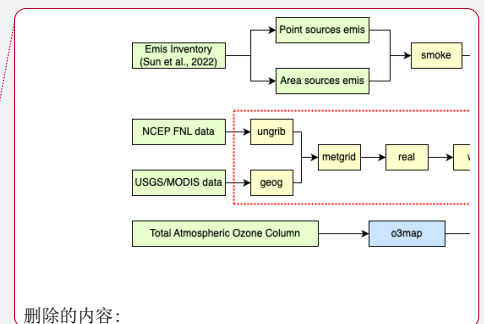
136 **Figure 1.** Framework of WRF-CAMx modeling system. The core modules have been  
 137 ported to MIPS and LoongArch CPU platforms. The core modules are framed by red  
 138 dashed line in the figure.

139 In Xi'an, China and Milan, Italy, the WRF-CAMx modelling system was applied,  
 140 enabling high-resolution hourly model output of pollutant concentration within specific  
 141 local urban areas (Pepe et al., 2016; Yang et al., 2020). The modeling system is widely  
 142 used to study the spatial-temporal variation of pollutant concentration and source  
 143 apportionment, analyze the contribution of regional transport to pollution and  
 144 investigate the impact of initial conditions and emissions on pollution simulation in key  
 145 regions such as the North China Plain, Sichuan Basin, and Fenwei Plain (Bai et al.,  
 146 2021; Zhen et al., 2023; Zhang et al., 2022; Xiao et al., 2021).

147

## 148 2.1 Description of WRF-CAMx modeling system

149 WRF and CAMx serve as the core components of the modeling system. WRF is a  
 150 mesoscale numerical weather prediction system designed for atmospheric research and  
 151 operational forecasting applications. Distinguished by its high temporal and spatial  
 152 resolution, WRF is suitable for multi-scale simulations of short-term weather forecast,  
 153 atmospheric process, and long-term climate, making it an essential tool in the  
 154 meteorological and atmospheric research communities (Powers et al., 2017). In the  
 155 modeling system, WRF provided gridded meteorological field data for air quality  
 156 model CAMx. The relative humidity, a meteorological variable used in result validation  
 157 is calculated using the wrf-python package (Official website: [https://wrf-  
 158 python.readthedocs.io](https://wrf-python.readthedocs.io), last access: October 2023). CAMx is an atmospheric pollutant



删除的内容:

删除的内容: '

删除的内容: Europe

删除的内容: developed

删除的内容: WRF is a high-resolution mesoscale model, which can be utilized for various purposes such as weather research and forecasting, physical parameterization scheme research, data assimilation and mesoscale climate simulation.

已移动(插入) [2]

删除的内容: Relative humidity

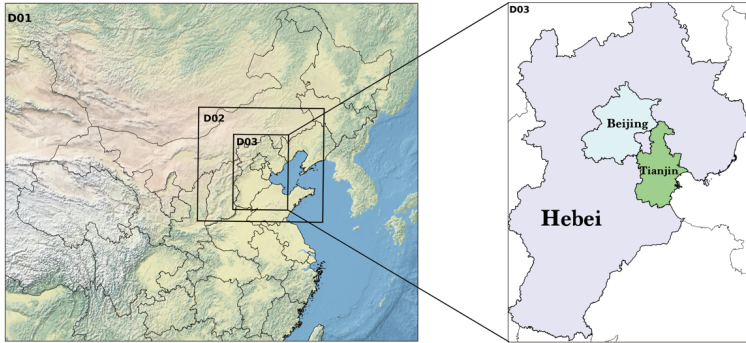
168 calculation model, which can be utilized for simulating and predicting the  
169 concentrations of various air pollutants. The WRF and CAMx models are distinguished  
170 by modularity and parallelism, using MPI in parallel computing, making them efficient  
171 (Skamarock et al., 2019; RAMBOLL ENVIRON Inc., 2014).

172 In the modeling system, the SMOKE model and cmaq2camx program are used to  
173 process emission data and provide model-ready gridded emission data for the CAMx  
174 model. The wrfcamx program converts the WRF results into meteorological input files  
175 which are compatible with CAMx. TUV is a radiation transfer model capable of  
176 producing clean sky photolysis rate input files for the chemical mechanisms in CAMx,  
177 and the o3map program prepares ozone column input files for TUV and CAMx. The  
178 icbcprep program prepares initial and boundary condition files for CAMx with the  
179 profile, and the effects of initial conditions have been studied by Xiao et al. (2021). The  
180 camx2ioapi program converts the CAMx output files into netCDF format following the  
181 Models-3/IO-API convention, and then uses NCL or other softwares to analyses the  
182 model results.

183

#### 184 **2.1.1 Model domain setup**

185 The model domain focusing on the Beijing-Tianjin-Hebei region has been set up  
186 in this study. The WRF model has three nested domains with horizontal resolutions of  
187 27km (D1), 9km (D2), and 3km (D3), as shown in Figure 2. The outer domain (D1)  
188 covers most parts of China, and the inner domain (D3) covers Beijing, Tianjin, and  
189 Hebei Province. The model domain is centered at (35°N, 110°E), with two true latitudes  
190 located at 20°N and 50°N. The vertical resolution of WRF is 34 vertical layers. The  
191 CAMx model has only one model domain, which is the innermost grid with a resolution  
192 of 3km (D3), mainly covering the Beijing-Tianjin-Hebei region. The vertical resolution  
193 of CAMx is 14 vertical layers, which is extracted from the WRF output files using the  
194 wrfcamx module, and the lower seven layers of CAMx are same as those in the WRF  
195 model.



196  
 197 **Figure 2.** The domains of three-level nested grids in the WRF-CAMx modelling system.  
 198 The respective horizontal resolutions are 27 km × 27 km (D1), 9 km × 9 km (D2), and  
 199 3 km × 3 km (D3).

200  
 201 **2.1.2 Model configuration**

202 Starting from 00:00 on November 3, 2020, until 24:00 on November 5, 2020, the  
 203 modelling system simulated the meteorological and air quality for a period of 72 hours.  
 204 In the research of Wang et al. in 2019, a 72h test case was set for the scientific validation  
 205 and performance evaluation of the chemistry transport models. A 72h case represents a  
 206 moderate-sized real scientific workload, which allows for simulating in a short time to  
 207 validate the results and assess computational efficiency on the MIPS and LoongArch  
 208 platforms. For the meteorological model, the global meteorological initial and boundary  
 209 fields for the WRF model are derived from the NCEP Global Final Reanalysis Data  
 210 (FNL), with a spatial resolution of 0.5° x 0.5° and a temporal resolution of 6 hours. And  
 211 the parameterization schemes of the WRF model used in the simulation case are shown  
 212 in Table 1.

213 For the air quality model, the meteorological files are provided by the WRF model  
 214 are used for the chemical transport module in CAMx. The emission inventory used in  
 215 the simulation case was obtained from Sun et al. (2022a). It contains basic emissions  
 216 from Sun et al. (2022b) and fugitive dust emission from bare ground surfaces. The  
 217 SMOKE model (v2.4) is used to process the emission inventory and provide gridded

已移动(插入) [1]

删除的内容: ,

删除的内容: testing

删除的内容: , and

删除的内容: validating

删除的内容: of the WRF-CAMx model on the MIPS platform

删除的内容: assessing

225 emissions for CAMx. The parameterization schemes of the CAMx model used in the  
 226 simulation case are shown in Table 2.

227

228 **Table 1.** Parameterization schemes of WRF in research case.

Parameterization process	Scheme
Microphysics	WSM3
Longwave radiation	RRTM
Shortwave radiation	Dudhia
Land surface	Noah
Planetary boundary layer	YSU
Cumulus parameterization	Kain-Fritsch(new Eta)

229

230 **Table 2.** Parameterization schemes of CAMx in research case.

Parameterization process	Scheme
Horizontal Diffusion	PPM
Vertical Diffusion	K-theory
Dry Deposition	Zhang03
Gas-phase chemical mechanism	CB05
Aqueous aerosol chemistry	RADM-AQ
Inorganic gas-aerosol partitioning	ISORROPIA

231

### 232 **2.1.3 Statistical indicators for model results**

233 To quantify the differences in the model results between the MIPS and benchmark  
 234 platform, three statistical indicators are used to analyze the differences of concentration  
 235 time series: Mean Absolute Error (MAE), Root Mean Square Error (RMSE), and Mean  
 236 Absolute Percentage Error (MAPE). The MAPE quantifies the deviation between  
 237 computational differences and simulated values. The smaller these indicators, the better  
 238 accuracy and stability of scientific computing of the modeling system on the MIPS  
 239 platform. The calculation formulas for these statistical indicators are provided in  
 240 equations (1) to (3).

241 
$$MAE = \frac{1}{n} \sum_{i=1}^n |MIPS(i) - Base(i)| \quad (1)$$

242 
$$RMSE = \left[ \frac{1}{n} \sum_{i=1}^n (MIPS(i) - Base(i))^2 \right]^{\frac{1}{2}} \quad (2)$$

243 
$$MAPE = \frac{1}{n} \sum_{i=1}^n \left| \frac{MIPS(i) - Base(i)}{MIPS(i)} \right| \times 100\% \quad (3)$$

已移动(插入) [3]



244 In the equations,  $n$  represents the number of grids in the domain.  $MIPS(i)$  represents the  
245 simulated value of a certain grid on the MIPS platform, and  $Base(i)$  represents the  
246 baseline value of a certain grid on the benchmark platform.

247

## 248 **2.2 MIPS and LoongArch CPU platforms description**

249 Loongson CPU platform was chosen for the porting work in the study. Currently,  
250 the Loongson processor family has three generations of CPU products, evolving from  
251 single-core to multi-cores architectures and from experimental prototypes to mass-  
252 produced industrial products (Hu et al., 2011). The Loongson-2 processor is a 64-bit  
253 general-purpose RISC processor series which is compatible with MIPS instruction set.  
254 It can be used in personal computers, mobile terminals, and various embedded  
255 applications, running many operating systems such as Linux and Android smoothly  
256 (Zhi et al., 2012). Wu et al. (2019) reports the application of the mesoscale model on  
257 Loongson 2F CPU platform. The Loongson-3 processor features a scalable multi-core  
258 architecture, targeting high-throughput data centers, high-performance scientific  
259 computing, and other applications, with the significant advantage of achieving a high  
260 peak performance-to-power ratio and striking a well-balanced trade-off between  
261 performance and power consumption (Hu et al., 2009).

262 The Loongson 3A series are multi-core processors designed for high-performance  
263 computers, featuring with high bandwidth, and low power consumption. The efficient  
264 design solution and the advantage of high energy efficiency ratio make servers based  
265 on Loongson CPUs highly competitive in performance, power consumption, and cost-  
266 effectiveness (Li et al., 2014; Wang et al., 2014). In this study, the Loongson platform  
267 uses the Debian Linux operating system, commercially known as Tongxin UOS  
268 (<https://www.uniontech.com>, last access: [January, 2024](#)), and the Loongson 3A4000  
269 processor, which is the first quad-core processor based on GS464v 64-bit  
270 microarchitecture in Loongson 3 Processor Family. The main technical parameters of  
271 Loongson 3A4000 CPU are shown in Table 3. Compared to previously released CPUs,  
272 the processor improves frequency and performance by optimizing on-chip interconnect  
273 and memory access path, integrating 64-bit DDR4 memory controller and on-chip

删除的内容: ↵

A lot of porting and optimization research work has been conducted to ensure the proper functioning of the high-performance mathematical library on Loongson platforms, resulting in improved computing performance, such as FFT (Fast Fourier Transform) (Guo et al., 2012; Li et al., 2011; Zhao et al., 2012). The porting and optimization efforts conducted on the multi-core Loongson processors have successfully demonstrated the stability and efficiency in the numerical computing applications. These results provide valuable technical references and rationality validation for the numerical model application on Loongson platform.

删除的内容: October 2023

287 security mechanism. The Loongson 3A6000 CPU platform uses Loongnix, the open-  
 288 source community edition operating system released by Loongson  
 289 (<https://www.loongson.cn/system/loongnix>, last access: January, 2024), and the latest  
 290 released Loongson 3A46000 processor, which is a quad-core processor based on LA664  
 291 microarchitecture. The main technical parameters of Loongson 3A6000 CPU are shown  
 292 in Table 3. The processor supports the LoongArch™ instruction set and hyper-threading,  
 293 and the performance has significantly improved compared to the previously released  
 294 processors (Hu et al., 2022).

删除的内容: <https://www>  
 带格式的: 默认段落字体, 字体: (默认) +西文正文 (DengXian), 五号  
 带格式的: 默认段落字体, 字体: (默认) +西文正文 (DengXian), 五号

295  
 296 **Table 3.** Main Parameters of Loongson 3A4000 CPU and Loongson 3A6000 CPU\*

Main Parameters	Loongson 3A4000 CPU	Loongson 3A6000 CPU
Main Frequency	1.8GHz-2.0GHz	2.0GHz-2.5GHz
Peak Computing Speed	128Gflops@2.0GHz	240Gflops
Transistor Technology	28nm	12nm
Number of Cores	4	4(Physical) 8(Logical)
Processor Cores	MIPS64 compatible Support 128/256-bit vector instructions	support LoongArch™ Support 128/256-bit vector instructions
High-speed I/O	2 x 16-bit HyperTransport 3.0 control	1 x HyperTransport 3.0 control
Typical Power Consumption	<30W@1.5GHz <40W@1.8GHz <50W@2.0GHz	38W@2.5GHz

删除的内容:  
 删除的内容: Loongson 3A4000 CPU

297 \*source: <https://www.loongson.cn>, last access: January, 2024.

删除的内容: Loongson 3A4000 CPU Main Parameters [1]  
 删除的内容: October 2023

299 **2.3 Benchmark platform description**

300 This study uses an X86 CPU platform as benchmark platform compared to the  
 301 MIPS and LoongArch CPU platforms. The benchmark platform is powered by Intel  
 302 Xeon E5-2697 v4 CPU, with strong floating-point performance and many technical  
 303 features such as Intel Turbo Boost Technology (Intel Inc., 2023). The Intel Xeon E5-  
 304 2697 v4 CPU has 18 cores, with 2.3GHz base frequency and 3.6GHz maximum Turbo  
 305 Boost frequency, 45 MB Intel Smart Cache and 145W design power consumption. The  
 306 operating system is CentOS Linux 7.4.1708. The main information for all platforms is

删除的内容: CPU platform  
 删除的内容: both

314 shown in Table 4.

315

316 **Table 4.** The comparison of main configuration between MIPS, LoongArch and X86  
317 platforms.

	<u>MIPS Platform</u>	<u>LoongArch</u> <u>Platform</u>	<u>X86 platform</u>
<u>CPU</u>	Loongson 3A4000	Loongson 3A6000	Intel Xeon E5-2697 v4
<u>Number of CPUs</u>	1	1	1
<u>Number of CPU</u> <u>cores</u>	4	8	18
<u>CPU Frequency</u>	1.8GHz	2.0Ghz	2.3GHz
<u>CPU instruction set</u>	MIPS64	LoongArch™	X86_64
<u>Operating system</u>	Tongxin UOS	Loongnix	CentOS Linux 7.4.1708
<u>Operating system</u> <u>kernel</u>	4.19.0-loongson-3-	4.19.0-19-	3.10.0-
<u>(Linux version)</u>	desktop	loongson-3	957.1.3.el7.x86_64

318

319

320 **2.4 The difference between MIPS, LoongArch and X86 platforms**

321 In this study, the numerical model's source code is written in Fortran, and  
322 commonly used compilers for X86 architecture include Intel Compiler, PGI and GNU  
323 Compiler. The compiler for MIPS platform is built using GCC 8.3 MIPS GNU/Linux  
324 cross-toolchain based on the open-source GNU Project, called MIPS GNU, and the  
325 latest version is 8.3. And the compiler for LoongArch platform is built using GCC 8.3  
326 LoongArch GNU/Linux cross-toolchain based on the open-source GNU Project, called  
327 LoongArch GNU, and the latest version is 8.3. The compiler for the benchmark  
328 platform is set to X86 GNU, and the version is also 8.3. Table 5 shows the differences  
329 between all platforms' GNU compilers in terms of applicable platforms. Compared to  
330 X86 GNU, the default compilation options of MIPS GNU compiler not only specify  
331 the platform architecture but also include additional instruction sets, such as atomic

带格式的: 居中

带格式的: 居中

带格式的: 居中

带格式的: 居中

带格式的: 居中

带格式的: 居中

带格式的: 居中

带格式的: 居中

删除的内容:   
MIPS Platform

删除的内容: the two

删除的内容: '

336 operation instruction set LLSC, shared library instruction set PLT, etc., which can  
 337 optimize target programs compiled by GNU for MIPS architecture and improve  
 338 computational efficiency. [And the default compilation options of LoongArch GNU  
 339 compiler not only specify the platform architecture but also include target  
 340 microarchitecture tuning option, which can also optimize target programs compiled by  
 341 GNU for LoongArch architecture.](#)

342 **Table 5.** Comparison of GNU compiler between MIPS, [LoongArch](#) and X86 CPU  
 343 platforms.

<u>Artitecture</u>	<u>MIPS64</u>	<u>LoongArch</u>	<u>x86_64</u>
<u>Compiler</u>	MIPS GNU Fortran	LoongArch GNU Fortran	X86 GNU Fortran
<u>Version</u>	8.3	8.3	8.3
<u>Target</u>	mips64el-linux-gnuabi64	loongarch64-linux-gnu	x86_64-redhat-linux
<u>Options (Architecture)</u>	-march=mips64r2 -mabi=64	-march=loongarch64 -mabi=lp64d	-march=x86-64 -mtune=generic
<u>Options (Instruction set)</u>	-mlisc -mplt - mmadd4	-mtune=loongarch64	/
<u>FLAGS(WRF)</u>	-fconvert=big-endian -frecord-marker=4 -ffree-line-length-none -O2 -ftree-vectorize -funroll-loops		
<u>FLAGS(CAMx)</u>	-fconvert=big-endian -frecord-marker=4 -ffixed-line-length-none -fno-align-commons -O2		

344 The WRF-CAMx modeling system depends on several scientific computing  
 345 libraries. Firstly, the general data format libraries netCDF and HDF5 are required to  
 346 store the large-scale gridded data for the modeling system. NetCDF is a self-describing  
 347 data format developed by NCAR/Unidata, primarily used for storing multidimensional  
 348 array data in fields like meteorology and earth sciences (UCAR/Unidata, 2021). HDF5  
 349 is a data format developed by HDF GROUP that supports complex data structures with  
 350 multiple data types and multi-dimensional datasets (The HDF Group, 2019). In this  
 351 study, netCDF-C (v4.8.1), netCDF-Fortran (v4.5.3), HDF5 (v1.12.1) and IOAPI (v3.1)  
 352 were successfully installed on MIPS [and LoongArch](#) platforms by building from their  
 353 sources, which are obtained from the official website.

354 The MPICH library is required to support parallel computing in the modeling  
 355 system. In order to fully utilize computing resources, the method of MPI message

删除的内容: **Artitecture** ... [3]

357 communication is used in WRF and CAMx model (Wu et al., 2012). MPICH is an  
358 open-source, portable parallel computing library for implementing the MPI standard  
359 (Amer et al., 2021). It supports inter-process communication and data exchange in the  
360 parallel computing environment. Similarly, this study successfully installed MPICH  
361 (v3.4) on MIPS [and LoongArch platforms](#) by building from its source. During the  
362 compilation and installation of the mentioned libraries above, the configure tool was  
363 used to check the basic information of the platform's CPU and compiler, and prepare  
364 for compatibility with platform before compilation, the GNU compiler is used to  
365 compile the source code of libraries, and the cmake tool is used to install the libraries.  
366 Additionally, the same runtime environment as MIPS platform was also built on the  
367 benchmark platform.

368

### 369 **3 Porting the WRF-CAMx modelling system on MIPS [and LoongArch](#)**

#### 370 **CPU platforms**

371 The simulation result is influenced by several factors including processor  
372 architecture, operating system, compiler, parallel environment, and scientific  
373 computing libraries. In order to ensure stability and accuracy of numerical simulation,  
374 the models should be adapted to the new runtime environment when porting across  
375 platforms. Additionally, various operating systems have different tools, software and  
376 libraries, which may impact the results of numerical simulations.

377 In this study, the runtime environment for WRF-CAMx modeling system was built  
378 on MIPS [and LoongArch platforms, including parallel computing libraries such as](#)  
379 [MPICH3 \(v3.4\) and data format libraries such as HDF5 \(v1.15.1\) and NETCDF \(C-](#)  
380 [v4.8.1, Fortran-v4.5.3\). These libraries do not support the architecture \(mips64el and](#)  
381 [LoongArch\) and GNU compiler of Loongson platform. Relevant information needs to](#)  
382 [be added to the free software config.guess and config.sub provided by GNU org. Part](#)  
383 [of the information is shown in subfigure a\) in Figure 3, which can help identify the](#)  
384 [platform architecture and system during the compilation and installation of libraries](#)  
385 [using Configure and Make tools.](#) The configuration files for making the models were

386 modified to fit the compilers of the Linux system on MIPS and LoongArch platforms.  
387 In order to verify the stability of scientific computing on MIPS and LoongArch  
388 platforms, a control experiment was set up on the benchmark platform, minimizing the  
389 impact of other factors on simulation results of both platforms.

删除的内容: UOS

390 The WRF v4.0 and CAMx v6.10 were successfully deployed on MIPS and  
391 LoongArch platforms through source code compilation and installation. In the WRF  
392 model, the default options for GNU compiler which are suitable for MIPS and  
393 LoongArch architecture CPUs are not provided in the configure file of the source code  
394 package, and it is necessary to incorporate architecture-specific settings for the model.  
395 For example, the architecture presets are stored in the configure.defaults file, but  
396 settings about the Loongson platform is not included. Specific architecture details,  
397 including CPU architecture, GNU compiler and compilation flags, need to be added,  
398 which can ensure the correct display of configuration during building WRF model, and  
399 part of information is shown in subfigure b) in Figure 3. Table 5 provides the detailed  
400 information added in the configure file, mainly about MIPS and LoongArch GNU  
401 Fortran. When compiling Fortran programs on MIPS and LoongArch platforms, the  
402 MIPS and LoongArch GNU Fortran and necessary compilation flags must be specified.  
403 These flags include common Fortran file format flags such as -fconvert=big-endian and  
404 -frecord-marker=4, as well as optimization flags such as -O2 -ftree-vectorize -funroll-  
405 loops. By specifying the appropriate compiler and flags for MIPS and LoongArch  
406 architectures, the configure tool will provide necessary settings to compile WRF.  
407 Correspondingly, when compiling WRF on the benchmark platform, the compilation  
408 flags are strictly consistent with those of MIPS and LoongArch CPU platforms, which  
409 ensures that differences in simulation results of two platforms are primarily attributed  
410 to the underlying hardware architecture rather than changes in compilation settings.

删除的内容: manually add information about the CPU architecture, GNU compiler, and compilation flags on MIPS platform

411 In the CAMx model, the makefile provides information about parallelism and  
412 compilers. Similarly, information about the CPU architecture, GNU compiler, and  
413 compilation flags on MIPS and LoongArch platforms also needs to be added in the  
414 makefile. For the detailed information added in the makefile, please refer to Table 5.  
415 Additionally, the code of CAMx was modified to make it run smoothly on MIPS and

420 LoongArch platform. Taking some function in the CAMx model for example, the model  
421 frequently uses the “write” function for formatted output. The format specifiers in the  
422 parameters consist of data types (I, F, E, A, X, etc.) followed by a character width. In  
423 the CAMx model, the format specifiers in the write function mostly default to character  
424 width, but there is a compilation issue with MIPS GNU, requiring character width  
425 descriptors. It is also essential to ensure consistency with the default precision. A  
426 specific example is illustrated in the figure below. A specific example is showed in in  
427 subfigure c) in Figure 3. So far, the WRF-CAMx model has been successfully compiled  
428 and installed on the MIPS and LoongArch platforms after modifications of the  
429 configuration files mentioned above.

a)

```

'''
loongarch32:Linux:*** | loongarch64:Linux:***
GUESS=$UNAME_MACHINE-unknown-linux-$LIBC
;;
'''
mips64el:Linux:***
GUESS=$UNAME_MACHINE-unknown-linux-$LIBC
;;

```

b)

```

#ARCH      Linux mips64  gfortran compiler with gcc #serial smpar dmpar dm+sm
#
DESCRIPTION = GNU ($SFC/$SCC)
DMPARALLEL  = # 1
OMP_CPP     = # -D_OPENMP
OMP         = # -fopenmp
OMPCC      = # -fopenmp
SFC         = gfortran
SCC         = gcc
CCOMP      = gcc
DM_FC      = mpiF90 -f90=$(SFC)
DM_CC      = mpicc -cc=$(SCC)
FC         = CONFIGURE_FC
CC         = CONFIGURE_CC
LD         = $(FC)
RWORDSIZE  = CONFIGURE_RWORDSIZE
PROMOTION  = #-fdefault-real-8
ARCH_LOCAL = -DNONSTANDARD_SYSTEM_SUBR -DWRP_USE_CLM
CFLAGS_LOCAL = -w -O3 -c
LDFLAGS_LOCAL =
CPLUSPLUSLIB =
ESMF_LDFLAG = $(CPLUSPLUSLIB)
FCOPTIM     = -O2 -ftree-vectorize -funroll-loops
FCREDUCEDOPT = $(FCOPTIM)
FCNDOPT     = -O0

```

c)

```

Before modification:
write (iout,'(a,2a)') ' spec','total [ug/m3]','c* [ug/m3] '
write (iout,'(i5,2e)') (idx(i),sctot(i),scsat(i),i=1,nsol)
write (iout,'(a,2e)') ' cpre,cpx ',cpre,cpx

After modification:
write (iout,'(a5,2a15)') ' spec','total [ug/m3]','c* [ug/m3] '
write (iout,'(i5,2e15.7)') (idx(i),sctot(i),scsat(i),i=1,nsol)
write (iout,'(a5,2e15.7)') ' cpre,cpx ',cpre,cpx

```

430  
431 Figure 3. Sample codes containing configure index, architecture-specific settings and  
432 functions in the WRF-CAMx model. Panel a) provides architecture information for  
433 configuration. Panel b) shows architecture-specific settings for WRF. Panel c)  
434 illustrates the sample code of functions in the CAMx before and after modification.

## 435 4 The differences of model results on the two platforms

### 436 4.1 Validation of the spatial distribution

437 A 72h simulation case has been designed to test the stability and availability of the  
438 WRF-CAMx modeling system on the MIPS CPU platform in Beijing. By analyzing the  
439 differences in simulation results and computing time, the accuracy and performance of

已上移 [1]: Starting from 00:00 on November 3, 2020, until 24:00 on November 5, 2020, the modelling system simulated the meteorological and air quality for a period of 72 hours, represents a moderate-sized real scientific workload, which allows for testing in a short time, and validating the results of the WRF-CAMx model on the MIPS platform and assessing computational efficiency.

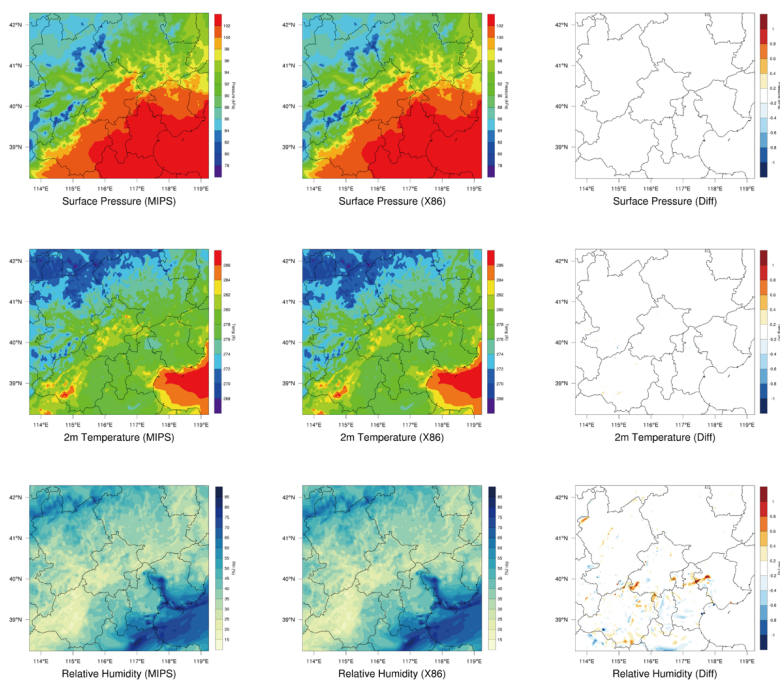


447 the modeling system on MIPS platform were evaluated, which further verifies the  
448 feasibility and stability of the modeling system after porting to the MIPS platform.

449 Common meteorological variables, including 2-meter temperature, land surface  
450 pressure, and relative humidity were selected to verify the WRF model results. Figure  
451 4 shows the spatial distribution of the four meteorological variables after 72 hours  
452 simulation on different platforms, as well as the absolute errors (AEs). The  
453 meteorological variables from the modeling system on the different platforms exhibit a  
454 generally consistent spatial distribution in the Beijing-Tianjin-Hebei regions shown in  
455 Figure 4.

删除的内容: 3

删除的内容: 3



456  
457 **Figure 4.** Spatial distribution of 2m temperature, surface pressure, relative humidity  
458 from WRF. Left column, MIPS platform. Middle, the X86 platform. Right, the  
459 differences between the MIPS and benchmark(X86) platform.

删除的内容: 3

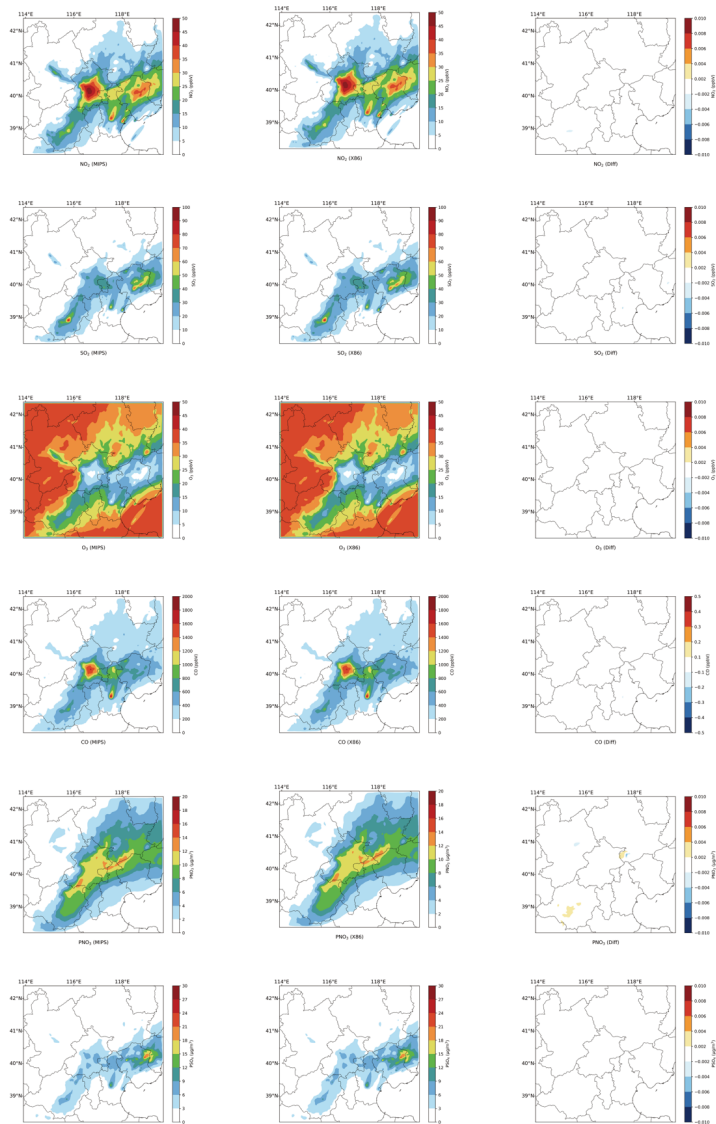
已上移 [2]: Relative humidity is calculated using the wrf-python package (Official website: <https://wrf-python.readthedocs.io>, last access: October 2023).

460  
461 Similarly, the NO<sub>2</sub>, SO<sub>2</sub>, O<sub>3</sub>, CO, PNO<sub>3</sub> and PSO<sub>4</sub> were selected to verify the

468 CAMx model results on the MIPS platform. Figure 5 shows the spatial distribution of  
469 the six species, as well as the absolute errors (AEs) between the two platforms after 72  
470 hours simulation. Simulating the 72h-case with four parallel processes using MPICH,  
471 CAMx takes about 9h on Loongson 3A4000 CPU and 2.6h on Intel Xeon E5-2697 v4  
472 CPU. As shown in Figure 5, the spatial distribution of air pollution concentrations from  
473 the different platforms is essentially consistent, appearing very similar visually.

删除的内容: 4

删除的内容: 4



476

477

**Figure 5.** Spatial distribution of NO<sub>2</sub>, SO<sub>2</sub>, O<sub>3</sub>, CO, PNO<sub>3</sub> and PSO<sub>4</sub> from CAMx on

478

MIPS and benchmark platform. Left column, MIPS platform. Middle, the X86 platform.

479

Right, the differences between the MIPS and benchmark(X86) platform.

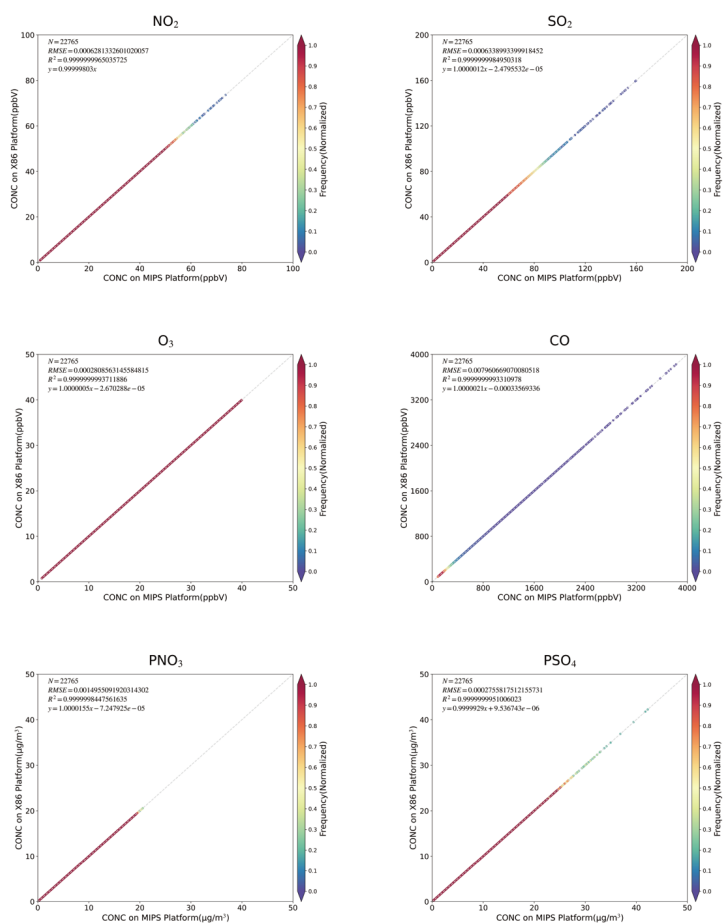
480

As shown in Figure 6, the scatter plots between the two platform, it can be seen

删除的内容: 4

删除的内容: 5

483 that for the total of 22,765 grids within the 145x157 simulation domain, the root mean  
 484 square errors (RMSEs) of the six species between the MIPS platform and benchmark  
 485 platform are close to 0.001, which is essentially 0. The linear regression model was  
 486 used to fit the scatters, and the regression slopes for each species are nearly 1, with  
 487 intercepts close to 0, and the R2 values used for the goodness of fit are nearly 1. The  
 488 fitted lines closely coincide with the “y=x” line, indicating that the differences between  
 489 the MIPS and X86 platform for each species are minimal to negligible.



490  
 491 **Figure 6.** Scatter of grid concentrations for NO<sub>2</sub>, SO<sub>2</sub>, O<sub>3</sub>, CO, PNO<sub>3</sub> and PSO<sub>4</sub> from  
 492 CAMx on the MIPS and benchmark platform. The density of scatters is represented by

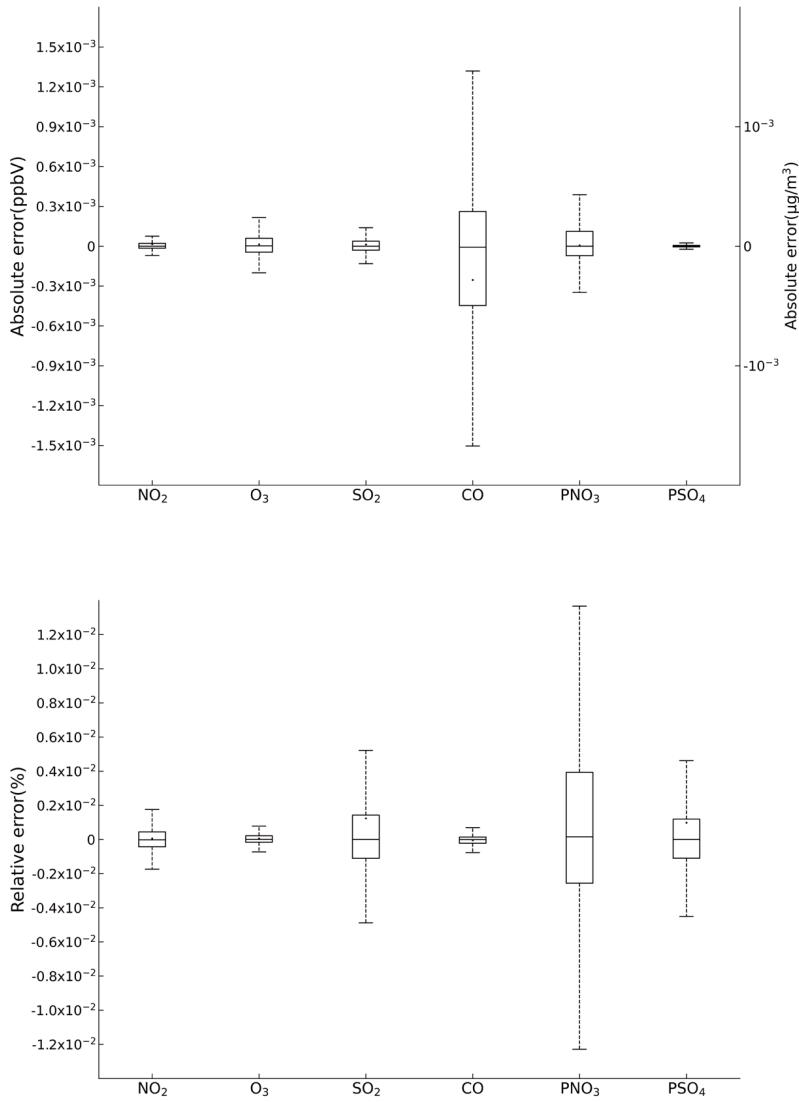
删除的内容: 5

494 the colors.

495 Figure 7 is the boxplots which show the absolute errors (AE) and relative errors  
496 (RE) of the six species between MIPS and benchmark platform. According to Figure 7,  
497 the absolute errors of the six species are generally in the range of  $\pm 10^{-3}$  ppbv (parts per  
498 billion by volume; the unit of NO<sub>2</sub>, SO<sub>2</sub>, O<sub>3</sub> and CO concentration) or  $\mu\text{g m}^{-3}$  (the unit  
499 of particle composition PNO<sub>3</sub> and PSO<sub>4</sub>), and the relative errors are generally in the  
500 range of  $\pm 0.01\%$ . Specially for CO, it exhibits more pronounced AEs compared to other  
501 species. In some grid boxes, the AEs between MIPS and benchmark platform exceed  
502 the range of  $\pm 10^{-3}$  ppbv, but they remain in the range of  $\pm 10^{-2}$  ppbv. In summary, there  
503 are some errors between the results of the modeling system on the MIPS and benchmark  
504 platform during the porting process. However, these errors are relatively minor  
505 compared to the numerical values. The reasons are attributed to the differences in the  
506 CPU architecture and compiler characteristics between the two platforms, such as data  
507 operations and precision running on different CPUs, which are primarily responsible  
508 for the observed errors.

删除的内容: 6

删除的内容: 6



511

512 **Figure 7.** The absolute errors and relative errors for NO<sub>2</sub>, SO<sub>2</sub>, O<sub>3</sub>, CO, PNO<sub>3</sub> and PSO<sub>4</sub>  
 513 concentration in all grids between the MIPS and benchmark platform.

514 Additionally, random grids in the domain were selected to assess the precision of  
 515 simulation results in localized regions. The positions of these grids were determined

删除的内容: 6

517 based on 32 observation stations in Beijing, and the nearest grid was determined using  
518 the Euclidean Shortest Distance in the domain. The station map is presented in Figure  
519 S1 in the Supplement. The Taylor diagram is used to assess the precision of  
520 concentrations for six species near the observation stations, and the scatters  
521 representing the six species at 32 stations are highly overlapping. Statistical parameters  
522 used in the Taylor diagram, such as the correlation coefficient (R) approaching 1,  
523 normalized standard deviation (NSD) and normalized root mean square error (NRMSE)  
524 approaching 0, indicate high precision of the simulation results at specific stations on  
525 the MIPS platform.

526

#### 527 **4.2 Validation of the temporal distribution from the two platform**

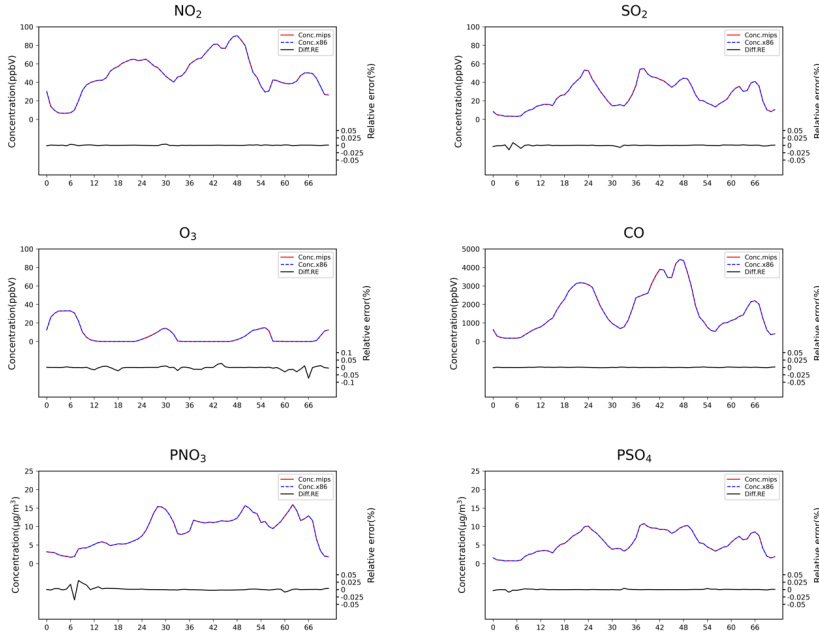
528 The time series of computational differences also be evaluated in this study.  
529 Random grid in the domain was selected to examine the hourly concentrations of the  
530 six species. Taking the example of the Beijing Olympic Center station (116.40°E,  
531 39.99°N) from the National Standard Air Quality (NSAQ) stations, the time series of  
532 hourly concentrations in the grid of the Beijing Olympic Center station and relative  
533 errors between the MIPS and benchmark platform over the 72-hour period were shown  
534 in Figure 8. As shown in Figure 8, it can be seen that the time series of the air pollutant  
535 concentrations were highly consistent between the two platforms. In the 72-hour period,  
536 the relative errors for NO<sub>2</sub>, SO<sub>2</sub>, CO and PSO<sub>4</sub> remain in ±0.025%. For PNO<sub>3</sub>, the  
537 relative errors remain in ±0.05%, and for O<sub>3</sub>, they remain in ±0.1%. This indicates that  
538 the errors caused by different architectures are within a reasonable range.

删除的内容:

删除的内容:

删除的内容: 7

删除的内容: 7



543  
544 **Figure 8.** Time-series of NO<sub>2</sub>, SO<sub>2</sub>, O<sub>3</sub>, CO, PNO<sub>3</sub> and PSO<sub>4</sub> concentrations and its  
545 relative errors (RE) at the Beijing Olympic Sports Center site between the MIPS and  
546 X86 platform. The red solid line and the blue dashed line, the CAMx model results on  
547 MIPS platform and X86 platform. The black solid line shows the relative errors (RE)  
548 between the MIPS and X86 platform.

549  
550 **Figure 9** shows the time series of the concentration and their statistical indicators,  
551 MAE, RMSE, and MAPE during the 72-hour simulation. As show in the figure, for  
552 NO<sub>2</sub>, SO<sub>2</sub>, O<sub>3</sub>, and PSO<sub>4</sub>, the MAEs are all below 10<sup>-3</sup> ppbv (µg m<sup>-3</sup>), and the RMSEs  
553 are all below 10<sup>-3</sup>. The MAEs for CO and PNO<sub>3</sub> are below 10<sup>-2</sup> ppbv (µg m<sup>-3</sup>), and the  
554 RMSEs for PNO<sub>3</sub> are below 10<sup>-2</sup>, while the RMSEs for CO are below 10<sup>-1</sup>. This is  
555 because that PNO<sub>3</sub> and CO have relatively higher background concentrations compared  
556 to the other species. The MAPE of PNO<sub>3</sub> concentration mainly ranging in 0-0.5%, while  
557 the MAPE of CO concentration has the lowest values below 0.001%, and the other  
558 species are in the range of 0-0.01%. Overall, the above time-series analysis verifies the  
559 accuracy and stability of the modeling system on the MIPS platform.

删除的内容: 7

已上移 [3]: To quantify the differences in the model results between the MIPS and benchmark platform, three statistical indicators are used to analyze the differences of concentration time series: Mean Absolute Error (MAE), Root Mean Square Error (RMSE), and Mean Absolute Percentage Error (MAPE). The MAPE quantifies the deviation between computational differences and simulated values. The smaller these indicators, the better accuracy and stability of scientific computing of the modeling system on the MIPS platform. The calculation formulas for these statistical indicators are provided in equations (1) to (3).<sup>4</sup>

$$MAE = \frac{1}{n} \sum_{i=1}^n |MIPS(i) - Base(i)| \quad (1)^{4}$$

$$RMSE = \left[ \frac{1}{n} \sum_{i=1}^n (MIPS(i) - Base(i))^2 \right]^{\frac{1}{2}} \quad (2)^{4}$$

$$MAPE = \frac{1}{n} \sum_{i=1}^n \left| \frac{MIPS(i) - Base(i)}{MIPS(i)} \right| \times 100\% \quad (3)^{4}$$

In the equations,  $n$  represents the number of grids in the domain.  $MIPS(i)$  represents the simulated value of a certain grid on the MIPS platform, and  $Base(i)$  represents the baseline value of a certain grid on the benchmark platform.<sup>4</sup>

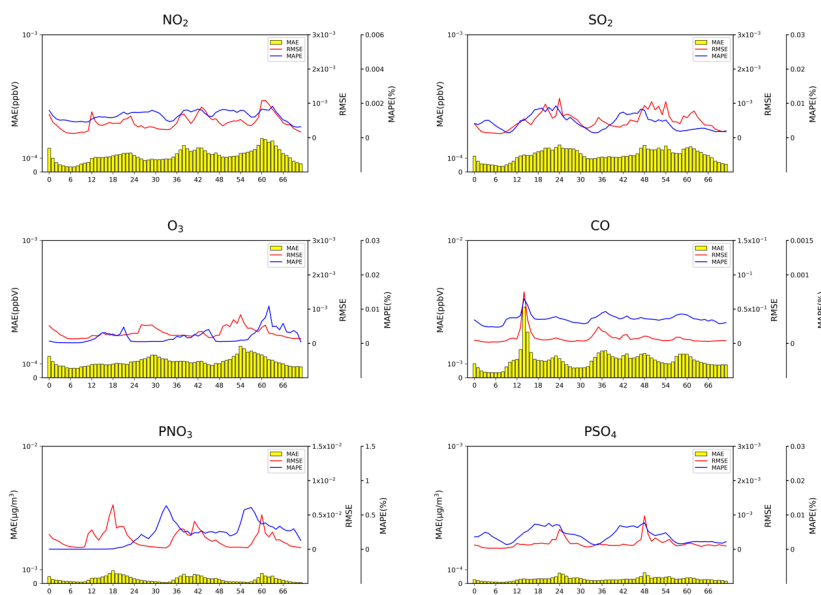
删除的内容:  $MAE = \frac{1}{n} \sum_{i=1}^n |MIPS(i) - Base(i)|$

删除的内容:  $RMSE = \left[ \frac{1}{n} \sum_{i=1}^n (MIPS(i) - Base(i))^2 \right]^{\frac{1}{2}}$

删除的内容:  $MAPE = \frac{1}{n} \sum_{i=1}^n \left| \frac{MIPS(i) - Base(i)}{MIPS(i)} \right| \times 100\%$

删除的内容: 8





586

587 **Figure 9.** Time series of MAEs, RMSEs and MAPEs for NO<sub>2</sub>, SO<sub>2</sub>, O<sub>3</sub>, CO, PNO<sub>3</sub> and  
 588 PSO<sub>4</sub> concentration in the 72h simulation. The yellow bar, the MAE. The red lines,  
 589 RMSE, the blue lines, MAPE.

删除的内容: 8

590

591 In this study, the evaluation method proposed by Wang et al. (2021) was also used  
 592 to assess the scientific applicability of the model results on the MIPS platform. The  
 593 Root Mean Square Errors (RMSEs) for NO<sub>2</sub>, SO<sub>2</sub>, O<sub>3</sub>, CO, PNO<sub>3</sub> and PSO<sub>4</sub>  
 594 concentration between the MIPS and benchmark platform were computed, along with  
 595 the standard deviations (stds) used to describe the spatial variation of species, and the  
 596 ratio of RMSE to std, as shown in Table 6. The differences of the four species between  
 597 the two platforms are negligible compared to their own spatial variations. Therefore,  
 598 the results on the MIPS platform meet the accuracy requirements for research purpose.

599

600 **Table 6.** RMSE, std, RMSE/std for NO<sub>2</sub>, SO<sub>2</sub>, O<sub>3</sub>, CO, PNO<sub>3</sub> and PSO<sub>4</sub>.

	Differences in results	Spatial variation	RMSE/std
	RMSE	std	
NO <sub>2</sub>	$6.3 \times 10^{-7}$	0.01	$5.9 \times 10^{-5}$

<b>O<sub>3</sub></b>	$2.8 \times 10^{-7}$	0.01	$2.5 \times 10^{-5}$
<b>SO<sub>2</sub></b>	$6.3 \times 10^{-7}$	0.02	$3.9 \times 10^{-5}$
<b>CO</b>	$7.9 \times 10^{-6}$	0.30	$2.6 \times 10^{-5}$
<b>PNO<sub>3</sub></b>	$1.5 \times 10^{-3}$	3.8	$3.9 \times 10^{-4}$
<b>PSO<sub>4</sub></b>	$2.7 \times 10^{-4}$	3.9	$6.9 \times 10^{-5}$

602

603 In fact, the differences in model results cannot be completely eliminated, primarily  
 604 due to the varying CPU architectures and compilers. In the practical applications,  
 605 compared with the errors arising from the inherent uncertainties of the modeling system  
 606 and the input data, the differences of model results between different platforms can even  
 607 be considered negligible. The comprehensive analysis demonstrates that the results of  
 608 the WRF-CAMx modeling system on the MIPS CPU platform are reasonable.

609

## 610 **5 The evaluation about computational performance**

611 Scientific computing involves a significant amount of floating-point operations,  
 612 and the floating-point computational capability is a crucial indicator for CPU  
 613 performance. In this study, the simulation case was configured to conduct parallel  
 614 computing tests on the MIPS, [LoongArch](#) and benchmark platform. These tests  
 615 included assessing the CPU's single-core performance with the non-parallel model and  
 616 the platform's parallel performance with the parallel model using multiple processes.  
 617 The time of CAMx model running simulation case for [24](#) hours in the modeling system  
 618 are shown in Figure [10](#). From the figure, it can be observed that under single-core  
 619 conditions, the computing capability of the MIPS platform for CAMx is approximately  
 620 one-third of the X86 benchmark platform, [and the LoongArch platform is slightly lower](#)  
 621 [than the X86 benchmark platform](#).

622 It's worth noting that the simulation time of the CAMx model for running with two  
 623 processes in parallel and running in non-parallel remains approximately consistent.  
 624 This is because the MPI used in CAMx is designed using a "master/slave" parallel  
 625 processing approach, and a process is allocated for input/output and message  
 626 communication during the runtime (Cao K et al., 2023). This process doesn't perform  
 627 any simulation in the model. Therefore, the time required for parallelism of two

删除的内容: 2

删除的内容: 9

630 processes is comparable to the non-parallelism, and in some cases, it might even be  
631 slightly longer due to the overhead of MPI communication. Compared to non-parallel,  
632 the speedup of the MIPS platform with four-process parallelism using MPICH3 is  
633 approximately 2.8, while using OpenMP is about 2.9. and the speedup of the  
634 LoongArch platform with four-process parallelism using MPICH3 is approximately 2.8,  
635 while using OpenMP is about 2.9. For the X86 benchmark platform, running with four  
636 processes in parallel using MPICH3 has a speedup of approximately 2.7.

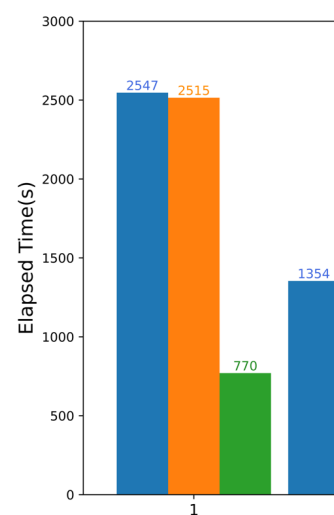
637 Additionally, the performance of the MIPS platform significantly decreases when  
638 the number of parallel processes exceeds 4. This is because the modeling system  
639 involves compute-intensive tasks. The Loongson 3A4000 CPU has four cores, and  
640 when the number of processes called by MPI matches the number of CPU cores, the  
641 CPU utilization can approach 100%. Further increasing the number of processes, the  
642 cores will compete for CPU resources, resulting in additional overhead and reduced  
643 computational efficiency. As for LoongArch platform, the performance slightly  
644 decreases when the number of parallel processes exceeds 4. The Loongson 3A6000  
645 CPU has four physical cores and eight logical cores, and when the number of processes  
646 called by MPI matches the number of physical cores, the computational load is evenly  
647 distributed across each core. Although the Loongson 3A6000 supports hyper-threading,  
648 further increasing the number of processes, CPU starts to schedule logical cores to  
649 allocate computational load. Thread scheduling will result in additional overhead and  
650 reduced computational efficiency. This explains why the elapsed time is slightly higher  
651 when CAMx running with 5 parallel processes compared to 4 parallel processes as  
652 shown in the section 2 of Supplementary Material.

删除的内容: .

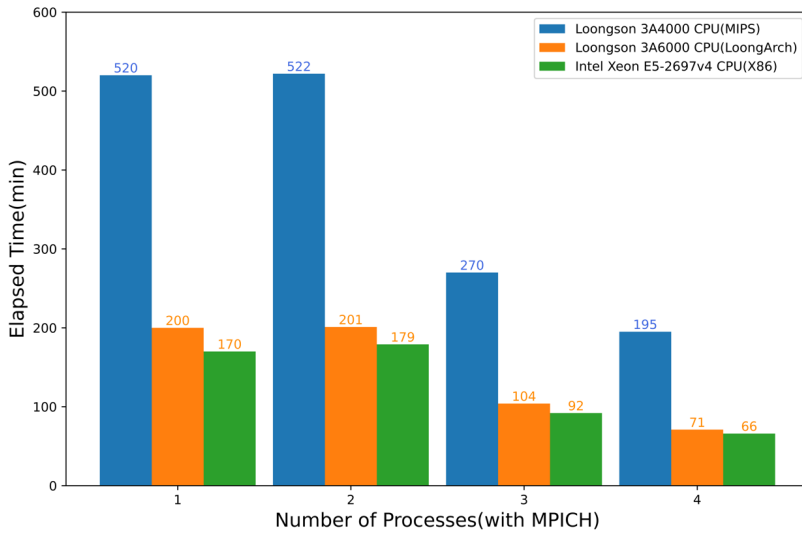
带格式的: 缩进: 首行缩进: 2 字符

删除的内容: reaches 5

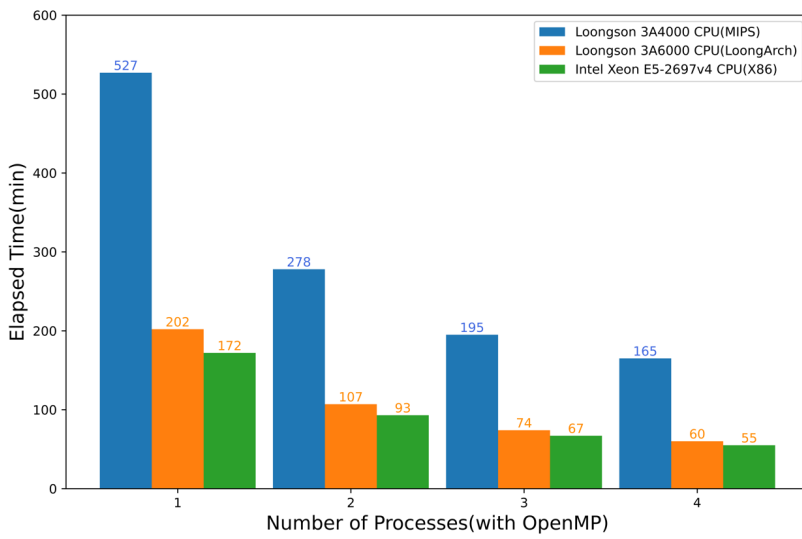
删除的内容: ↵



删除的内容:



657



658

659 **Figure 10.** Elapsed time of CAMx model running simulation case with MPICH and  
 660 OpenMP for 24 hours on the MIPS, LoongArch and benchmark platforms.

删除的内容: 9

删除的内容: 2

661

662 In the recent years, the Loongson CPUs have been continuously upgraded.  
 663 Compared to the previous generations of products, the performance of Loongson CPUs  
 664 has shown significant improvement. Wu et al. (2019) simulated a nested domain

删除的内容: the Loongson 3A4000 CPU

668 covering Beijing for 48 hours using the MM5 model on the Loongson 3A quad-core  
669 CPU platform. The results showed that the computational capacity of the Loongson 3A  
670 platform for the MM5 model is approximately equivalent to around 1/12 of the Intel  
671 Core 2 Q8400 quad-core CPU, which was released in the same year. In the study of  
672 Luo et al. (2011), a comparison between Loongson 3A and Intel i5 was made by running  
673 NPB benchmark on each platform. The results shows that the performance of the 3A is  
674 nearly one-tenth of that of the i5. The rapid development of Loongson CPUs has  
675 provided a strong hardware foundation for the application of numerical simulation and  
676 scientific computing on MIPS and LoongArch architecture CPU platforms. Based on  
677 the performance evaluation of WRF-CAMx modeling system on Loongson 3A4000  
678 and Loongson 3A6000 platform, it could be found that the computing capability nearly  
679 tripled while maintaining similar power consumption. The adaptation and optimization  
680 of the models based on RISC CPUs will also be an important research direction in the  
681 future. Many factors influencing parallel performance, such as computing scale, I/O,  
682 multiprocessor, etc., will be considered to evaluate on platforms with stronger  
683 performance and more processors in the future.

删除的内容: MIPS

684

## 685 **6 Conclusion**

686 This study describes the application of the WRF-CAMx model on the MIPS CPU  
687 platform. The platform used in this study is Loongson 3A4000 quad-core CPU with the  
688 main frequency of 1.8-2.0GHz, which can offer a peak operational speed of 128GFlops.

删除的内容: 2.0GHz

删除的内容: offering

689 It is equipped with the MIPS GNU compiler. The benchmark platform used the Intel  
690 Xeon E5-2697 v4 CPU along with the same version of X86 GNU compiler. Based on  
691 the characteristics of CPU architecture and compiler, this study has successfully  
692 completed the construction of runtime environment for the WRF-CAMx modeling  
693 system. The application of an air quality modelling system based on WRF-CAMx was  
694 successfully tested using a 72-hour simulation case in the Beijing-Tianjin-Hebei region.

695 The results showed that the spatial distribution of the meteorological variables and  
696 air pollutant species was nearly identical, with relative errors in the range of  $\pm 0.1\%$ .

700 Statistically, the maximum MAEs of major species ranged from  $10^{-3}$  to  $10^{-2}$  ppbv ( $\mu\text{g}$   
701  $\text{m}^{-3}$ ), the maximum RMSEs ranged from  $10^{-2}$  to  $10^{-1}$  ppbv ( $\mu\text{g} \text{m}^{-3}$ ), and the MAPEs  
702 remained within 0.5%, that the differences caused by the architectures and compilers  
703 were within a reasonable range. Simulating a 2h-case with four parallel processes using  
704 MPICH, CAMx takes about 15.2min on Loongson 3A4000 CPU and 4.8 min on Intel  
705 Xeon E5-2697 v4 CPU. In terms of single-core CPU performance, the single-core  
706 computing capability of Loongson 3A4000 CPU for the WRF-CAMx modeling system  
707 is about one-third of Intel Xeon E5-2697 v4 CPU.

708 Currently, Loongson Technology has **focused on** the LoongArch architecture and  
709 it has been used in the **latest** product. It is foreseeable that the LoongArch architecture  
710 will lead to more significant performance improvements. In the future, as the numerical  
711 models become more complex and computational scales become larger, more models  
712 will be tested on high-performance computing platforms equipped with the LoongArch  
713 architecture CPUs.

714  
715 **Code and data availability.** The source codes of CAMx version 6.10 are available at  
716 <https://camx-wp.azurewebsites.net/download/source> (ENVIRON, 2023). The datasets  
717 related to this paper and the **binary executable files of CAMx for MIPS and LoongArch**  
718 CPUs are available online via ZENODO (<https://doi.org/10.5281/zenodo.10722127>).

719  
720 **Supplement.** The supplement related to this article is available on-line.

721  
722 **Author contributions.** ZB and QW conducted the simulation and prepared the materials.  
723 QW planned and organized the project. ZB and QW completed the porting and  
724 application of the model for MIPS **and LoongArch** CPUs. YS collected and prepared  
725 the emission data for the simulation. ZB, QW, KC, and HC participated in the  
726 discussion.

727  
728 **Acknowledgements.** The National Key R&D Program of China (2020YFA0607804)  
729 and the Beijing Advanced Innovation Program for Land Surface funded this work. The

删除的内容: introduced

删除的内容: which is compatible with MIPS,

删除的内容: next-generation

删除的内容: , the 3A5000 CPU (Hu et al., 2022)

删除的内容: CAMx codes

删除的内容: <https://zenodo.org/records/10297970>

736 research is supported by the High Performance Scientific Computing Center (HSCC)  
737 of Beijing Normal University.

738

739 **Competing interests.** The contact author has declared that none of the authors has any  
740 competing interests.

741

## 742 **References**

- 743 Amer, A., Balaji, P., Bland, W., Gropp, W., Guo, Y., Latham, R., Lu, H., Oden, L., Pena, A. J.,  
744 Raffanetti, K., Seo, S., Si, M., Thakur, R., Zhang, J., and Zhao, X.: MPICH User's Guide  
745 Version 3.4, available at: <https://www.mpich.org/static/downloads/3.4/mpich-3.4-userguide.pdf>,  
746 2021.
- 747 Appel, K. W., Napelenok, S. L., Foley, K. M., Pye, H. O. T., Hogrefe, C., Luecken, D. J., Bash, J.  
748 O., Roselle, S. J., Pleim, J. E., Foroutan, H., Hutzell, W. T., Pouliot, G. A., Sarwar, G., Fahey, K.  
749 M., Gantt, B., Gilliam, R. C., Heath, N. K., Kang, D., Mathur, R., and Schwede, D. B.: Description  
750 and evaluation of the Community Multiscale Air Quality (CMAQ) modeling system version 5.1,  
751 Geoscientific Model Development, 10, 1703–1732, <https://doi.org/10.5194/gmd-10-1703-2017>,  
752 2017.
- 753 Appel, K. W., Bash, J. O., Fahey, K. M., Foley, K. M., Gilliam, R. C., Hogrefe, C., Hutzell, W. T.,  
754 Kang, D., Mathur, R., Murphy, B. N., Napelenok, S. L., Nolte, C. G., Pleim, J. E., Pouliot, G. A.,  
755 Pye, H. O. T., Ran, L., Roselle, S. J., Sarwar, G., Schwede, D. B., Sidi, F. I., Spero, T. L., and  
756 Wong, D. C.: The Community Multiscale Air Quality (CMAQ) model versions 5.3 and 5.3.1:  
757 system updates and evaluation, Geoscientific Model Development, 14, 2867–2897,  
758 <https://doi.org/10.5194/gmd-14-2867-2021>, 2021.
- 759 Bai, X., Tian, H., Liu, X., Wu, B., Liu, S., Hao, Y., Luo, L., Liu, W., Zhao, S., Lin, S., Hao, J., Guo,  
760 Z., and Lv, Y.: Spatial-temporal variation characteristics of air pollution and apportionment of  
761 contributions by different sources in Shanxi province of China, Atmospheric Environment, 244,  
762 117926, <https://doi.org/10.1016/j.atmosenv.2020.117926>, 2021.
- 763 Cao, K., Wu, Q., Wang, L., Wang, N., Cheng, H., Tang, X., Li, D., and Wang, L.: GPU-HADVPPM  
764 V1.0: a high-efficiency parallel GPU design of the piecewise parabolic method (PPM) for  
765 horizontal advection in an air quality model (CAMx V6.10), Geosci. Model Dev., 16, 4367–4383,  
766 <https://doi.org/10.5194/gmd-16-4367-2023>, 2023.
- 767 Chen, H. S., Wang, Z. F., Li, J., Tang, X., Ge, B. Z., Wu, X. L., Wild, O., and Carmichael, G. R.:  
768 GNAQPMS-Hg v1.0, a global nested atmospheric mercury transport model: model description,  
769 evaluation and application to trans-boundary transport of Chinese anthropogenic emissions,  
770 Geoscientific Model Development, 8, 2857–2876, <https://doi.org/10.5194/gmd-8-2857-2015>,  
771 2015.
- 772 George, A. D.: An overview of RISC vs. CISC, in: [1990] Proceedings. The Twenty-Second  
773 Southeastern Symposium on System Theory, The Twenty-Second Southeastern Symposium on  
774 System Theory, Cookeville, TN, USA, 436–438, <https://doi.org/10.1109/SSST.1990.138185>,  
775 1990.

776 Hennessy, J., Jouppi, N., Przybylski, S., Rowen, C., Gross, T., Baskett, F., and Gill, J.: MIPS: A  
777 microprocessor architecture, SIGMICRO Newsl., 13, 17–22,  
778 <https://doi.org/10.1145/1014194.800930>, 1982.

779 Hu, W., Wang, J., Gao, X., Chen, Y., Liu, Q., and Li, G.: Godson-3: A Scalable Multicore RISC  
780 Processor with x86 Emulation, IEEE Micro, 29, 17–29, <https://doi.org/10.1109/MM.2009.30>,  
781 2009.

782 Hu, W., Zhang, Y., and Fu, J.: An introduction to CPU and DSP design in China, Sci. China Inf. Sci.,  
783 59, 1–8, <https://doi.org/10.1007/s11432-015-5431-6>, 2016.

784 Hu, W., Gao, X., and Zhang, G.: Building the software ecosystem for the Loongson instruction set  
785 architecture, Information and Communications Technology and Policy, 43–48, 2022 (in Chinese).

786 Hu, W.-W., Gao, Y.-P., Chen, T.-S., and Xiao, J.-H.: The Godson Processors: Its Research,  
787 Development, and Contributions, J. Comput. Sci. Technol., 26, 363–372,  
788 <https://doi.org/10.1007/s11390-011-1139-2>, 2011.

789 Intel Inc.: Intel® 64 and IA-32 Architectures Software Developer’s Manual, Volume 1: Ba  
790 sic Architecture, available at: [https://www.intel.com/content/www/us/en/developer/articles/te  
791 chnical/intel-sdm.html](https://www.intel.com/content/www/us/en/developer/articles/technical/intel-sdm.html), 2023.

792 Li, L., Chen, Z., and Wang, S.: Power Consumption and Analysis of Server Based on Loongson  
793 CPU No. 3, Information Technology & Standardization, 46–50, 2014 (in Chinese).

794 Liu, Y., Ye, K., and Xu, C.-Z.: Performance Evaluation of Various RISC Processor Systems: A Case  
795 Study on ARM, MIPS and RISC-V, in: Cloud Computing – CLOUD 2021, Cham, 61–74,  
796 [https://doi.org/10.1007/978-3-030-96326-2\\_5](https://doi.org/10.1007/978-3-030-96326-2_5), 2022.

797 Luo, Q., Kong, C., Cai, Y., and Liu, G.: Performance Evaluation of OpenMP Constructs and Kernel  
798 Benchmarks on a Loongson-3A Quad-Core SMP System, in: 2011 12th International Conference  
799 on Parallel and Distributed Computing, Applications and Technologies, 2011 12th International  
800 Conference on Parallel and Distributed Computing, Applications and Technologies, 191–196,  
801 <https://doi.org/10.1109/PDCAT.2011.66>, 2011.

802 Mallach, E. G.: RISC: Evaluation and Selection, Journal of Information Systems Management, 8,  
803 8–16, <https://doi.org/10.1080/07399019108964978>, 1991.

804 Michalakes, J., Chen, S., Dudhia, J., Hart, L., Klemp, J., Middlecoff, J., and Skamarock, W.:  
805 Development of a next-generation regional weather research and forecast model, in:  
806 Developments in Teracomputing, WORLD SCIENTIFIC, 269–276,  
807 [https://doi.org/10.1142/9789812799685\\_0024](https://doi.org/10.1142/9789812799685_0024), 2001.

808 MIPS Technology Inc.: MIPS Architecture For Programmers Volume I-A, available at:  
809 <https://www.mips.com/products/architectures/mips64>, 2014.

810 Pepe, N., Pirovano, G., Lonati, G., Balzarini, A., Toppetti, A., Riva, G. M., and Bedogni, M.:  
811 Development and application of a high resolution hybrid modelling system for the evaluation of  
812 urban air quality, Atmospheric Environment, 141, 297–311,  
813 <https://doi.org/10.1016/j.atmosenv.2016.06.071>, 2016.

814 Powers, J. G., Klemp, J. B., Skamarock, W. C., Davis, C. A., Dudhia, J., Gill, D. O., Coen, J. L.,  
815 Gochis, D. J., Ahmadov, R., Peckham, S. E., Grell, G. A., Michalakes, J., Trahan, S., Benjamin,  
816 S. G., Alexander, C. R., Dimego, G. J., Wang, W., Schwartz, C. S., Romine, G. S., Liu, Z., Snyder,  
817 C., Chen, F., Barlage, M. J., Yu, W., and Duda, M. G.: The Weather Research and Forecasting  
818 Model: Overview, System Efforts, and Future Directions, Bulletin of the American  
819 Meteorological Society, 98, 1717–1737, <https://doi.org/10.1175/BAMS-D-15-00308.1>, 2017.

删除的内容: Guo, L. and Liu, Y.: Efficient Implementation of FFT on Loongson 3A CPU, Journal of Chinese Computer Systems, 33, 594–597, 2012 (in Chinese).<sup>d</sup>

删除的内容: Li, L., Chen, Y.-J., Liu, D.-F., Qian, C., and Hu, W.-W.: An FFT Performance Model for Optimizing General-Purpose Processor Architecture, J. Comput. Sci. Technol., 26, 875–889, <https://doi.org/10.1007/s11390-011-0186-z>, 2011.<sup>d</sup>



828 RAMBOLL ENVIRON Inc.: CAMx User's Guide Version 6.1, available at: [https://camx-](https://camx-wp.azurewebsites.net/Files/CAMxUsersGuide_v6.10.pdf)  
829 [wp.azurewebsites.net/Files/CAMxUsersGuide\\_v6.10.pdf](https://camx-wp.azurewebsites.net/Files/CAMxUsersGuide_v6.10.pdf), 2014.

830 Shi, Z.: Technology comparison and research of RISC and CISC, China Science and Technology  
831 Information, 131–132, 2008 (in Chinese).

832 Skamarock, C., Klemp, B., Dudhia, J., Gill, O., Liu, Z., Berner, J., Wang, W., Powers, G., Duda, G.,  
833 Barker, D., and Huang, X.: A Description of the Advanced Research WRF Model Version 4,  
834 <https://doi.org/10.5065/1dfh-6p97>, 2019.

835 Sun Y.: Research on the contribution of soil fugitive dust in Beijing based on satellite identification  
836 and numerical simulation technology, Master, Beijing Normal University, <https://etdlib.bnu.edu.cn>,  
837 2022a.

838 Sun, Y., Wu, Q., Wang, L., Zhang, B., Yan, P., Wang, L., Cheng, H., Lv, M., Wang, N., and Ma, S.:  
839 Weather Reduced the Annual Heavy Pollution Days after 2016 in Beijing, *Sola*, 18, 135–139,  
840 <https://doi.org/10.2151/sola.2022-022>, 2022b.

841 The HDF Group: HDF5 User's Guide Version 1.1, available at:  
842 <https://portal.hdfgroup.org/display/HDF5/HDF5+User+Guides>, 2019.

843 UCAR/Unidata: NetCDF User's Guide Version 1.1, available at: <https://docs.unidata.ucar.edu/nug> ,  
844 2021.

845 [Wang, H., Lin, J., Wu, Q., Chen, H., Tang, X., Wang, Z., Chen, X., Cheng, H., and Wang, L.: MP](https://doi.org/10.5194/gmd-12-749-2019)  
846 [CBM-Z V1.0: design for a new Carbon Bond Mechanism Z \(CBM-Z\) gas-phase chemical](https://doi.org/10.5194/gmd-12-749-2019)  
847 [mechanism architecture for next-generation processors, \*Geoscientific Model Development\*, 12,](https://doi.org/10.5194/gmd-12-749-2019)  
848 [749–764, <https://doi.org/10.5194/gmd-12-749-2019>, 2019.](https://doi.org/10.5194/gmd-12-749-2019)

849 Wang, K., Gao, C., Wu, K., Liu, K., Wang, H., Dan, M., Ji, X., and Tong, Q.: ISAT v2.0: an  
850 integrated tool for nested-domain configurations and model-ready emission inventories for WRF-  
851 AQM, *Geoscientific Model Development*, 16, 1961–1973, [https://doi.org/10.5194/gmd-16-1961-](https://doi.org/10.5194/gmd-16-1961-2023)  
852 [2023](https://doi.org/10.5194/gmd-16-1961-2023), 2023.

853 Wang, P., Jiang, J., Lin, P., Ding, M., Wei, J., Zhang, F., Zhao, L., Li, Y., Yu, Z., Zheng, W., Yu, Y.,  
854 Chi, X., and Liu, H.: The GPU version of LASG/IAP Climate System Ocean Model version 3  
855 (LICOM3) under the heterogeneous-compute interface for portability (HIP) framework and its  
856 large-scale application, *Geosci. Model Dev.*, 14, 2781–2799, [https://doi.org/10.5194/gmd-14-](https://doi.org/10.5194/gmd-14-2781-2021)  
857 [2781-2021](https://doi.org/10.5194/gmd-14-2781-2021), 2021.

858 Wang, S., Li, L., and Chen, Z.: The Test and Analysis on Memory Access Performance Based on  
859 Loongson CPU, *Information Technology & Standardization*, 32–36, 2014 (in Chinese).

860 Wang, Z., Xie, F., Wang, X., An, J., and Zhu, J.: Development and Application of Nested Air Quality  
861 Prediction Modeling System, *Chinese Journal of Atmospheric Sciences*, 778–790,  
862 <http://dx.doi.org/10.3878/j.issn.1006-9895.2006.05.07>, 2006.

863 Wu, Q. and Cheng, H.: Transplantation and application of mesoscale mode on Loongson CPU  
864 platform, *Journal of Beijing Normal University (Natural Science)*, 55, 11–18,  
865 <https://doi.org/10.16360/j.cnki.jbnuns.2019.01.002>, 2019.

866 Wu, Q., Xu, W., Shi, A., Li, Y., Zhao, X., Wang, Z., Li, J., and Wang, L.: Air quality forecast of  
867 PM10 in Beijing with Community Multi-scale Air Quality Modeling (CMAQ) system: emission  
868 and improvement, *Geoscientific Model Development*, 7, 2243–2259,  
869 <https://doi.org/10.5194/gmd-7-2243-2014>, 2014.

870 Wu, Y., Xu, G., Zhao, Y., and Tan, Y.: Parallel Processing on WRF Meteorological Data Using  
871 MPICH, in: 2012 Sixth International Conference on Internet Computing for Science and

872 Engineering, 2012 Sixth International Conference on Internet Computing for Science and  
873 Engineering, titleTranslation., 262–265, <https://doi.org/10.1109/ICICSE.2012.12>, 2012.

874 Xiao, H., Wu, Q., Yang, X., Wang, L., and Cheng, H.: Numerical study of the effects of initial  
875 conditions and emissions on PM2.5 concentration simulations with CAMx v6.1: a Xi'an case  
876 study, *Geoscientific Model Development*, 14, 223–238, [https://doi.org/10.5194/gmd-14-223-](https://doi.org/10.5194/gmd-14-223-2021)  
877 [2021](https://doi.org/10.5194/gmd-14-223-2021), 2021.

878 Yang, X., Xiao, H., Wu, Q., Wang, L., Guo, Q., Cheng, H., Wang, R., and Tang, Z.: Numerical study  
879 of air pollution over a typical basin topography: Source appointment of fine particulate matter  
880 during one severe haze in the megacity Xi'an, *Science of The Total Environment*, 708, 135213,  
881 <https://doi.org/10.1016/j.scitotenv.2019.135213>, 2020.

882 Zhang, Y., Bocquet, M., Mallet, V., Seigneur, C., and Baklanov, A.: Real-time air quality forecasting,  
883 part I: History, techniques, and current status, *Atmospheric Environment*, 60, 632–655,  
884 <https://doi.org/10.1016/j.atmosenv.2012.06.031>, 2012.

885 Zhang, Z., Wang, X., Cheng, S., Guan, P., Zhang, H., Shan, C., and Fu, Y.: Investigation on the  
886 difference of PM2.5 transport flux between the North China Plain and the Sichuan Basin,  
887 *Atmospheric Environment*, 271, 118922, <https://doi.org/10.1016/j.atmosenv.2021.118922>, 2022.

888 Zhen, J., Guan, P., Yang, R., and Zhai, M.: Transport matrix of PM2.5 in Beijing-Tianjin-Hebei and  
889 Yangtze River Delta regions: Assessing the contributions from emission reduction and  
890 meteorological conditions, *Atmospheric Environment*, 304, 119775,  
891 <https://doi.org/10.1016/j.atmosenv.2023.119775>, 2023.

892 Zhi, Y. and Xu, J.: Android transplantation and analysis based on Loongson, in: 2012 International  
893 Conference on Information Management, Innovation Management and Industrial Engineering,  
894 2012 International Conference on Information Management, Innovation Management and  
895 Industrial Engineering, 59–61, <https://doi.org/10.1109/ICIII.2012.6339777>, 2012.

删除的内容: Zhao, M., Zhang, Y., Liu, Y., Li, Y., and Yan, S.: Comparison and Analysis of Three Types of FFT Adaptive Libraries on Loongson 3A, *Computer Science*, 39, 281–285, 2012 (in Chinese).<sup>4</sup>

第 10 页: [1] 删除的内容

Zehua Bai

2024/2/28 03:22:00

第 11 页: [2] 删除的内容

Zehua Bai

2024/2/28 03:33:00

第 12 页: [3] 删除的内容

Zehua Bai

2024/2/28 03:50:00